Indian Journal of Advances in Chemical Science

Article

Synthesis, Crystal Structure Refinement, and Morphological Study of Bioactive Material: Strontium and Iron-Substituted Nano-Hydroxyapatite: $Ca_{10-x}M_x(PO_4)_6(OH)_2$ (M=Sr and Fe and $0 \leq x \leq 0.1$)

O. P. Shrivastava[1]*, Ramesh C. Deka[1], Rashmi Chourasia[2] and Rasnadevi[1]

[1]Department of Chemical Science, Tezpur University, Tezpur, Assam, India, [2]Department of Chemistry, Dr H.S. Gour University, Sagar, MP, India

ABSTRACT

Nano-hydroxyapatite (HA) is a bioactive and important material well known for several applications. Rietveld refinement and structural analysis of X-ray powder diffraction patterns have been investigated to understand the effect of Sr and Fe substitution on the structural properties of bioactive material $Ca_{10-x}M_x(PO_4)_6(OH)_2$ or $Ca_{5-x}M_x(PO_4)_3(OH)$ where M=Sr and Fe and x=0.05). The crystal chemistry of Sr- and Fe-substituted HA phases has been investigated using General Structure Analysis System programming. Sr- and Fe-substituted HA phases crystallize in the space group P 63/m; Z=2. Powder diffraction data have been subjected to Rietveld refinement to arrive at a satisfactory structural convergence of R-factors. The expected overall decrease of the lattice constants in the samples is explained in terms of local lattice distortions. The unit cell volume and polyhedral distortion increase with a rise in the size of loaded cation in the HA matrix. Scanning electron microscopy, transmission electron microscopy, and energy-dispersive X-ray analysis provide evidence of Sr and Fe in the HA matrix.

Key words: Bioactive nanomaterial, Hydroxyapatite, X-ray diffraction, General structure analysis system, Structure refinement, Fourier transform infrared, Scanning and transmission electron microscopy.

1. BACKGROUND

Main mineral component of bones and teeth, calcium hydroxyapatite (HA), belongs to the apatite family. HA group of compounds appears of high interest in the field of biomaterials because they represent a compatible inorganic component of natural bones and can be directly bond to bones *in vivo*. HA is usually applied as bone filling material, but by introducing cations into this compound, new applications could be feasible. One of them is to use it as a drug delivery material due to its biocompatibility, degradation, and dissolution characteristics and non-toxic nature [1-8]. Localized hyperthermia shows a promise as a treatment modality for tumor eradication [9]. In recent years, HA has been investigated as magnetic material for cancer treatment. It is reported that heating cells up to 42–46°C result in the death of cancer cells and this can be done by releasing the magnetic nanoparticles with AC magnetic field. HA has several other applications in the medical and engineering fields, and its further modification is needed to meet the requirements of recent applications [10,11]. Other advantage of HA structure is its flexibility to the substitution of ions. The general chemical formula is $M_5(YO_4)_3X$ where M=monovalent cations (such as Na^+ or K^+) or divalent cations (such as Ca^{2+}, Sr^{2+}, Ba^{2+}, Cd^{2+}, Pb^{2+}, Fe^{2+}, and Co^{2+}) or trivalent cations (such as Fe^{3+} and La^{3+}). X=OH^-, F^-, Cl^-, Br^-, or CO_3^{2-} and YO_4=PO_4, VO_4, SiO_4, and AsO_4 [11]. The hexagonal unit cell of HA contains ten cations distributed between two crystallographic sites: Four on type (1) sites and six on type (2) sites. Ca(1) ions are surrounded by nine oxygen atoms (three O(1), three O(2), and three O(3)). Ca(2) ions present are surrounded by six oxygen atoms such as one O(1), one O(2), four O(3), and one OH^- ion. Literature reveals that the substitution of ions in the crystal structures of HA substantially affects its physical and biological properties. Various papers have been recently published on the continuous improvement of properties of HA focusing on limitations to load-bearing applications on physical properties [12]. Li *et al.* reported the synthesis and cytocompatibility of Mn- and Fe-doped HA nanoparticles [13]. The application of HA depends on the crystal shape, size, morphology, crystallinity, thermal stability, and solubility, all of which are strongly influenced by the fabrication route [14]. Thus, the present communication aims to investigate the structure of hydrothermally synthesized Sr- and Fe-modified calcium HA nanophases through quantification of crystal data.

2. METHODS

2.1. Hydrothermal Synthesis of $Ca_{5-x}M_x(PO_4)_3OH$(M=Sr and Fe and x=0.05) Phases

Synthesis of unsubstituted hydroxyy apatite and Sr and Fe substituted hydroxy apatite nanophases: Apatites were synthesized by dropwise addition of aqueous solution of dipotassium hydrogen phosphate (KH_2PO_4) to a solution of calcium nitrate ($Ca(NO_3)_2.4H_2O$). Stoichiometric quantities of the starting materials have been dissolved in minimum amount of water to keep the Ca:P ratio 1.67 in case of pure HA. In case of strontium- and iron-substituted HA, appropriate quantity of solution of strontium nitrate and ferrous ammonium sulfate was added to keep strontium and iron at x=0.05 and overall molar ratio Ca+M/P=1.67 (M=Sr and Fe). The pH was maintained at

***Corresponding author:**
E-mail: dr_ops11@rediffmail.com

ISSN NO: 2320-0898 (p); 2320-0928 (e)
DOI: 10.22607/IJACS.2019.701001

Received: 24th December 2018;
Accepted: 10th January 2019

9.4 by continuous dropwise addition of ammonia solution. The entire precipitate was transferred to a 50 ml Teflon lined par vessel which was heated in an oven at 180°C for 72 h. After this period, the entire content was taken out, filtered, and washed several times to remove the unreacted reactants if any. The phase pure product was dried at 120°C, powdered, and analyzed by X-ray powder diffraction.

2.2. Characterization

Powder XRD spectra were recorded at room temperature, on a substituted Pan analytical diffractometer (Xpert-Pro) machine using Cu Kα=1.5406 Å radiation source operating at 40 kV and 30 mA. The diffraction patterns were collected over a 2θ, ranging from 10° to 90° with an incremental step size of 0.02 using flat plane geometry. The acquisition time was set at 2 s for each scan. The recorded powder XRD data were then used in subsequent modeling techniques. The microscope analysis started with scanning electron microscopy (SEM) with the aim to reveal the shape and the size of the synthesized particles. The samples were dispersed in water by means of an ultrasound bath and examined on a Zeiss SEM. A further structural analysis based on exploring the individual nanostructures was performed by TECNAI G2 20S (200KV) transmission electron microscopy (TEM) equipped with TIA (FEI imaging software), EMMENU4, EMTOOLS.

The sample was prepared by dispersing the powder in acetone using an ultrasonic bath and subsequently dropping the suspension on a lacey carbon film supported by a 300-mesh copper grid. Images were obtained with the aim of identifying the crystallographic orientations and the crystallinity of the single-crystal nanorods. Selected area electron diffraction (SAED) was also recorded and interlayer spaces were measured on different locations. Fourier-transform infrared (FTIR) spectroscopy was employed to determine the chemical functionality of Sr- and Fe-doped HA. The potassium bromide (KBr) disk technique was used for analysis using 2 mg of Sr and Fe HA powder compacted with 200 mg of KBr under hydraulic pressure. All the spectra were measured using Perkin Elmer (Spectrum Version 10.43) infrared spectrometer with a resolution of 4.00 cm^{-1} at room temperature, which covers the wave number range of 4000–400 cm^{-1} to evaluate the functional groups of the samples.

Table 1: Crystallographic data for $Ca_{5-x}M_x(PO_4)_3OH$ (M=Sr, Fe, and x=0.05) at room temperature.

Structure: Hexagonal; space group; P 63/m; Z=2		
Parameters	**Sr**	**Fe**
Lattice constants		
a=b	9.41557 (33)	9.40749 (10)
c	6.87647 (23)	6.87157 (11)
α=β=90°, γ=120°		
Rp	0.0430	0.0554
Rwp	0.0586	0.0806
$R_{expected}$	0.0387	0.0425
RF^2	0.06671	0.07508
Volume of unit cell ($Å^3$)	527.947 (30)	526.665 (10)
S (GoF)	1.522	1.91
Unit cell formula weight	1009.388	1006.211
Density-$_{ray}$	3.175 g/cm^3	3.173 g/cm^3

$$R_p = \frac{\sum y_i(obs) - y_i(cal)}{\sum y_i(Obs)} R_{wp} = \left\{ \frac{\sum w_i (y_i(obs)^2 - y_i(cal))^2}{\sum w_i (y_i(obs))^2} \right\}^2 R_e$$

$$= [(N - P) / \sum w_i Y^2_{oi}]^{1/2} S = R_{wp} / R_{exp}$$

$y_{i(o)}$ and $y_{i(c)}$ are observed and calculated intensities at profile point i, respectively. w_i is a weight for each step i. N is the number of parameters refined

3. RESULTS AND DISCUSSION

3.1. Rietveld Refinement and Crystal Structure Modeling from Powder XRD Data

The intensities and positions of the diffraction pattern of the title phases matched fairly with the reported standard pattern of parent HA which gives several prominent reflections between 2θ = 25.8 and 60.0 (Figure 1) [15]. Sr- and Fe-substituted HAs crystallize in hexagonal system. The space group P63/m was chosen while checking the symmetry by the LEPAGE method using the CHECKCELL program [16]. The structure of the synthetic phases has been refined by Rietveld method [17] using General Structure Analysis System [18] software, which allows determination of crystal structure, refinement of atomic coordinates, site occupancies, and atomic displacement parameters as well as profile parameters (lattice constants, peak shape, peak height, instrument parameters, and background). The structure refinement leads to rather good fit between the experimental and calculated XRD patterns (Figure 2) and yields acceptable reliability factors: RF^2, Rp, and Rwp (Table 1) [19]. The final atomic coordinates and isotropic thermal parameters (Table 2), interatomic distances and polyhedral distortion index (Table 3), bond angles (Table 4),

Table 2: Refined atomic coordinates of $Ca_{5-x}M_x(PO_4)_3OH$ (M=Sr, Fe, and x=0.05) sample at room temperature.

Atom	x	y	z	Occupancy	U_{iso} ($Å^2$) (Sr)	U_{iso} ($Å^2$) (Fe)
Ca1	0.33333	0.66667	0.0027	0.975	0.00825	0.00917
Fe	0.33333	0.66667	0.0027	0.025	0.00825	0.00917
Ca2	0.24556	0.99045	0.25	1.0	0.00825	0.00917
P	0.39789	0.36805	0.25	1.0	0.0065	0.00852
O1	0.32471	0.48617	0.25	1.0	0.02973	0.00852
O2	0.58721	0.45947	0.25	1.0	0.02973	0.01575
O3	0.34094	0.25385	0.06994	1.0	0.02973	0.01575
O4	0.0	0.0	0.25	1.0	0.02973	0.01575
H	0.0	0.0	0.0	1.0	0.48304	0.05683

U_{iso}: Isotropic thermal parameter

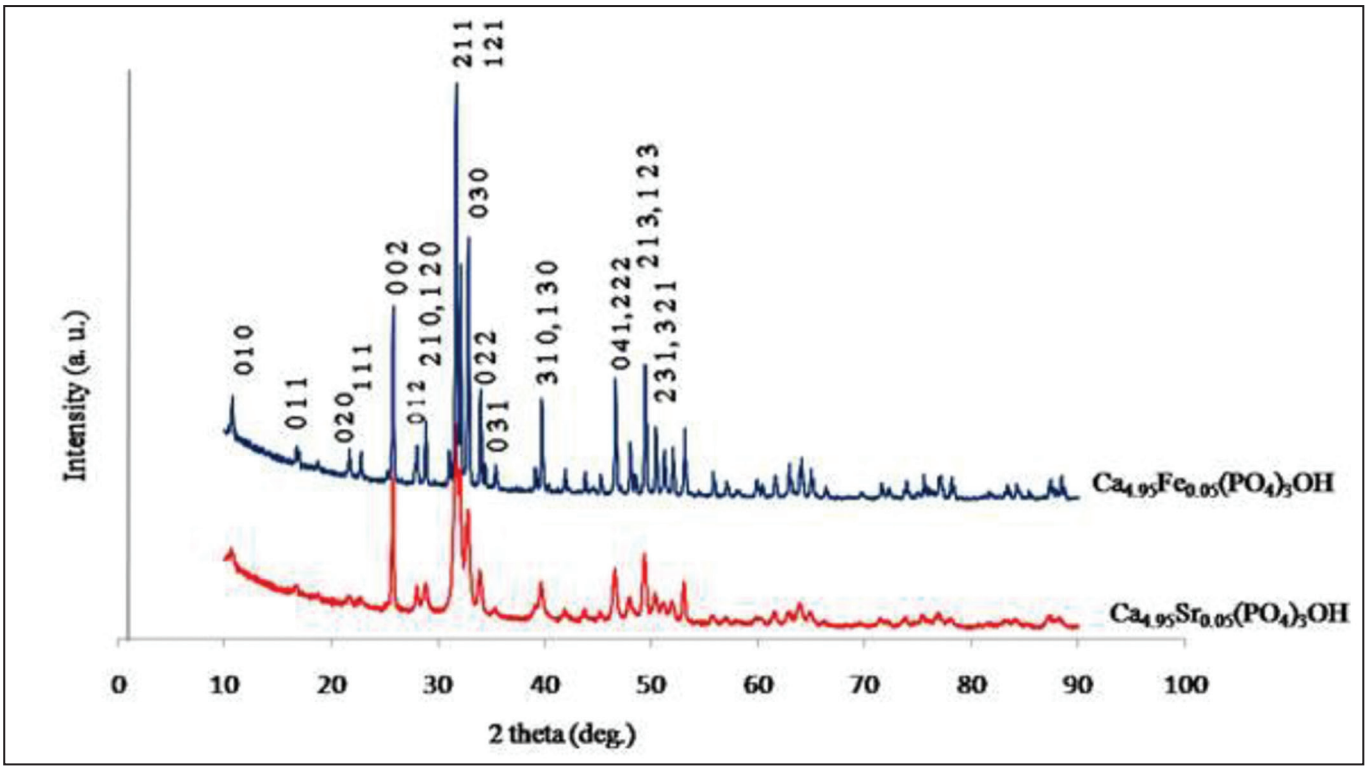

Figure 1: Powder X-ray diffraction pattern of Ca_5-x$Mx(PO_4)_3OH$(M=Sr, Fe and x=0.05) samples along with their prominent reflections.

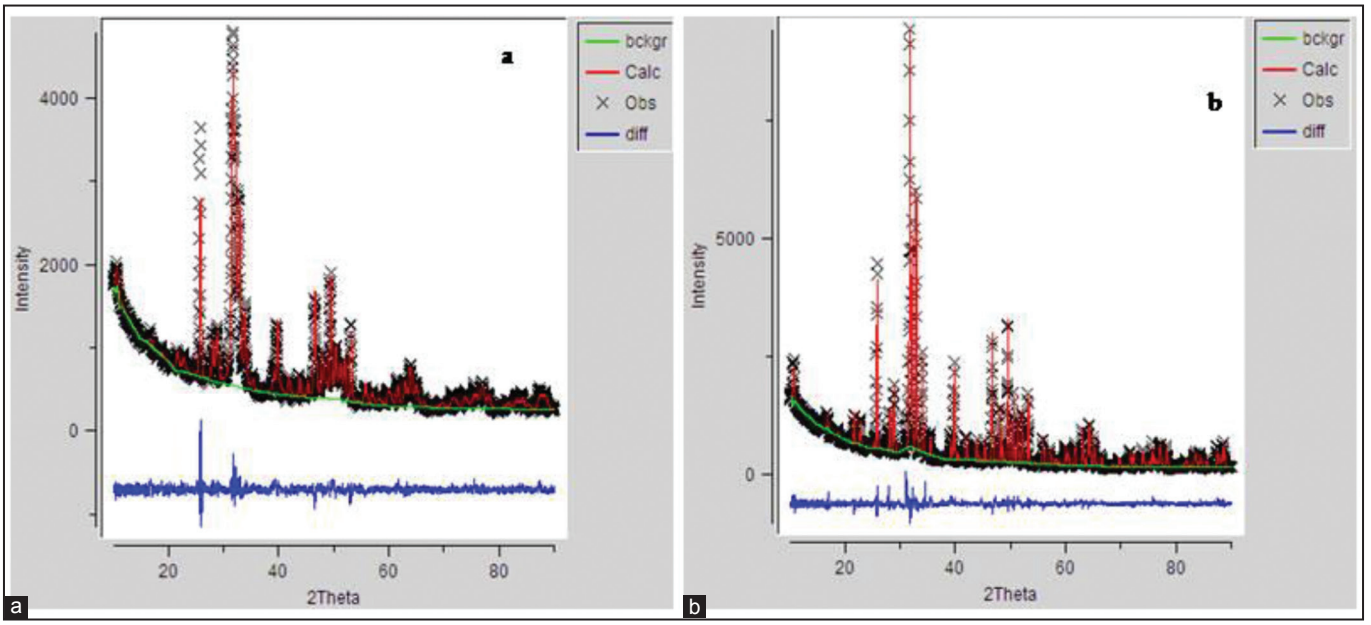

Figure 2: Rietveld refinement patterns of (a) $Ca_{4.95}Sr_{0.05}(PO_4)_3OH$ (b) $Ca_{4.95}Fe_{0.05}(PO_4)_3OH$ compounds. The 'x' are the raw X-ray diffraction data, and the overlapping continuous line is the calculated pattern. The curve at the bottom is the difference in the observed and calculated intensities in the same scale.

h, k, l planes, d-spacing, and intensity data along with observed and calculated structure factors (Appendix 1) have been reported in this communication. Figures 3a and b illustrate the DIAMOND projection of three-dimensional balls and stick structure of the proposed model of the materials showing the position and interconnectivity of PO_4 tetrahedrons and $Ca(1)O_9/SrO_9/FeO_9$ and $Ca(2)O_7$ polyhedrons. Figure 4 shows the PLATON projection of the molecular structure depicting the interlinking of $Ca(1)O_9$, $Ca(1)O_7$, and PO_4 through a bridge oxygen atom. Crystallite size along prominent reflecting planes for Sr- and Fe-substituted HA phases has been determined using the Scherrer's equation [20]. The size varies between 9 and 101 nm (Table 5).

3.2. Microstructure Analysis

The surface morphology of Fe-HA specimen has been investigated by SEM. The polycrystalline powder aggregated into flaky agglomerates

Table 3: Interatomic bond distances (Å) and polyhedral distortion (Δ) in polycrystalline $Ca_{5-x}M_x(PO_4)_3OH$ (M=Sr, Fe, and x=0.05) phases.

Bond-distance	Sr	Fe
Ca(1)/Fe–O(1)	2.37673(6)	2.374870(20)
Ca(1)/Fe–O(2)	2.37670(6)	2.374870(20)
Ca(1)/Fe–O(3)	2.37667(6)	2.374870(20)
	2.42449(6)	2.422590(20)
	2.42455(6)	2.422590(20)
	2.42450(6)	2.422590(20)
	2.81434(9)	2.811930(30)
	2.81424(9)	2.811930(30)
	2.81431(9)	2.811930(30)
Ca(2)–O(1)	2.66136(9)	2.659070(30)
Ca(2)–O(2)	2.40714(8)	2.405070(30)
Ca(2)–O(3)	2.50261(7)*2	2.500550(20)*2
Ca(2)–O(3)	2.33160(7)*2	2.329900(30)*2
Ca(2)–O(4)	2.35833(8)	2.356310(30)
P(1)–O(1)	1.57417(5)	1.572790(20)
P(1)–O(2)	1.54404(5)	1.542720(20)
P(1)–O(3)	1.54926(4)	1.548090(20)
P(1)–O(3)	1.54927(4)	1.548090(20)
Polyhedral distortion (Δ)		
$Ca(1)O_9$	8.0×10^{-3}	15×10^{-3}
$Ca(2)O_7$	51.3×10^{-4}	51.5×10^{-4}
PO_4	8.85×10^{-5}	8.78×10^{-5}

Δ=1/nΣ{(Ri-Rm)/(Rm)}2 where n=4, 7, and 9 for four, seven, and nine coordination, respectively

with grains of size 100–200 nm (Figure 5a). The compositional distributions in the grains and grain boundaries of Fe-HA have been measured by energy-dispersive X-ray (EDAX) analysis. The EDAX spectrum shows that Fe enters crystallo-chemically in the HA matrix (Figure 5b). The crystallographic planes and ordered arrangement of atoms in Sr-HA and Fe-HA are visible in the TEM image. In TEM, Sr-HA phase was observed in the form of needle-shaped nanorods (Figures 6a-c). To determine the particle size of the powder, measurements were taken along the length and width of several particles and the average of these measurements was calculated. The particle size of the powder was found to be distributed in the range 12–139 nm, while Fe-HA was observed in the form of spherical geometry with particles of 86–101 nanodimensions (Figures 7a-c). Simultaneously, the crystallite size was also determined using Scherrer's equation, where the broadening of a peak is expressed as full width at half maxima in the recorded XRD pattern. The results were found to be in line with the TEM investigations (Table 5). The SAED pattern (Figures 6d and 7d) of the Sr- and Fe-substituted HA nanopowders shows concentric rings in the diffraction pattern, which confirms the polycrystalline nature of the phases. Crystallographic planes and ordered arrangement of atoms are visible in the electron microscopy images.

3.3. FTIR Analysis

FTIR scanning spectra of Sr-HA and Fe-HA systems prepared by hydrothermal route are found to be very similar to those found in the literature [21-23]. Evolutions of these well-developed peaks indicate good crystallinity after hydrothermal treatment. Both the samples show bands corresponding to HA, which are confirmed by FTIR spectra. The characteristic bands for PO_{43-} appear at 470, 568, 602, 964, 1041, and 1093 cm^{-1} [24-26]. The sharp peaks located at 3571 cm^{-1} and 632 cm^{-1} correspond to the structural stretching vibration and deformation mode of OH, respectively. The strong doublet band or shoulder at

Table 4: O-M-O bond angles (deg.) of polycrystalline $Ca_{5-x}M_x(PO_4)_3OH$ (M=Sr, Fe and x=0.05) sample.

O-M-O Bond angles	M
	Sr
O1-Ca1-O1	74.4589 (22), 74.4583 (22), 74.4595 (22)
O1-Ca1-O2	155.7427 (6), 123.7519 (15), 94.0793 (27), 94.0804 (27), 155.7398 (6), 123.7558 (15)
O1-Ca1-O3	141.9990 (8), 68.4565 (14), 87.7200 (8)
O2-Ca1-O2	74.3046 (22), 74.3046 (22), 74.3044 (22)
O2-Ca1-O3	56.00590 (20), 123.4102 (18), 68.08800 (20)*2,56.00770 (20)
O3-Ca1-O3	116.92040 (30), 116.91830 (30), 116.92130 (30)
O1-Ca2-O2	102.6466
O1-Ca2-O3	149.7958 (12), 71.8651 (8)*2,149.7959 (12)
O1-Ca2-O4	106.9602
O2-Ca2-O3	73.84950 (20)*2,87.58580 (10)*2,
O2-Ca2-O4	150.3932
O3-Ca2-O3	136.5137 (4)*2,77.9863 (20)* 2,59.3071 (24),141.3246 (17)
O3-Ca2-O4	80.50800 (10)*2,101.4721 (5)*2
	Fe
O1-Ca1-O1	74.4518 (9)*3, 74.4530 (9)
O1-Ca1-O2	123.7579 (6)*, 94.0851 (11), 155.74020 (30), 155.74451 (30), 123.7565 (6), 94.0873 (11) 94.0884 (11), 155.74170 (30), 123.7604 (6),
O1-Ca1-O3	87.72040 (30), 141.99831 (30), 68.4586 (6), 68.4585 (6), 87.72310 (30), 141.99609 (30) 141.99660 (30), 68.4606 (6), 87.72230 (30)
O2-Ca1-O2	74.2981 (9), 74.2990 (9), 74.2979 (9)
O2-Ca1-O3	123.4046 (8), 68.08940 (10), 56.00730 (10), 56.00640 (10),123.4059 (8), 68.08750 (10), 68.08770 (10), 56.00820 (10), 123.4053 (8),116.91960 (10),116.91750 (10), 116.92040 (10)
O1-Ca2-O2	102.6466
O1-Ca2-O3	149.7923 (5)*2, 71.86760 (30)*2
O1-Ca2-O4	106.9602, 150.3932
O2-Ca2-O3	73.85010 (10)*2, 87.5861*2
O3-Ca2-O3	136.51500 (20)*2, 77.9803 (8)*2, 141.3298 (7)
O3-Ca2-O4	80.5083*2, 101.47060 (20)*2
O1-P-O2	113.4091
O1-P-O3	111.62090 (30)*2
O2-P-O3	106.81880 (20)*2
O3-P-O3	106.1153 (11)

960^{-1}–1100 cm^{-1} was assigned to asymmetric P-O stretching and bending vibration of the phosphate group (PO_{43-}). The ν_1 PO_4 stretch occurs at 961cm^{-1}, while ν_2 and ν_3 vibrations are observed at 1030 and 1090 cm^{-1}, respectively. The characteristic sharp bands at about 471–474 cm^{-1} (weak) and 570–601cm^{-1} (doublet) also represent PO_{43-} vibrations. A small band at around 1650 cm^{-1} was possibly due to absorbed water (bending mode) which is absent in case of Fe-HA (Figure 8).

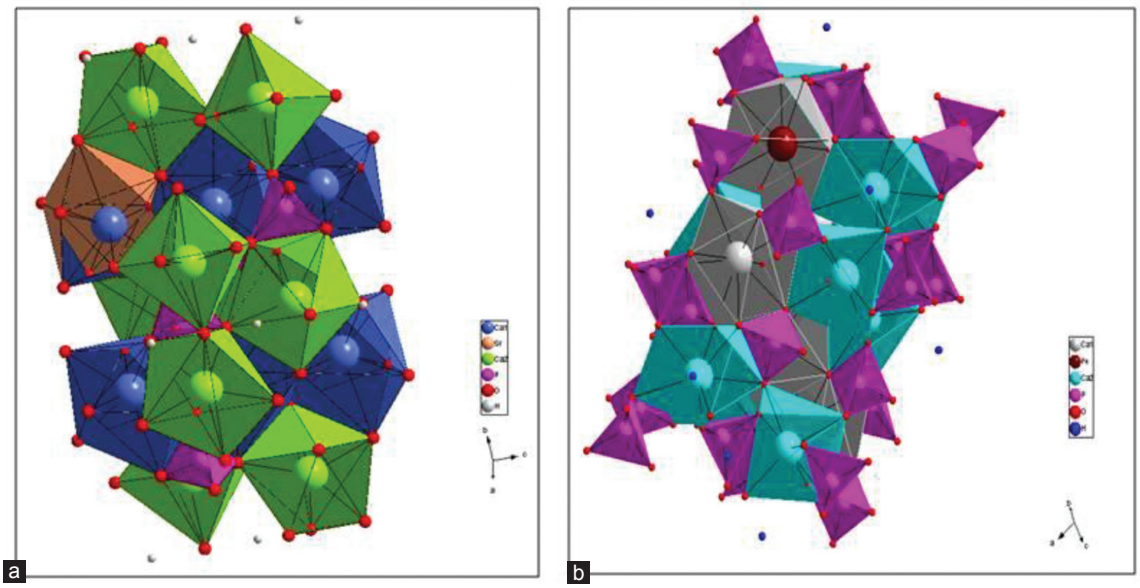

Figure 3: DIAMOND view of coordination sites of Ca, P and H in (a) $Ca_{4.95}Sr_{0.05}(PO_4)_3OH$ and (b) $Ca_{4.95}Fe_{0.05}(PO_4)_3OH$ compound respectively.

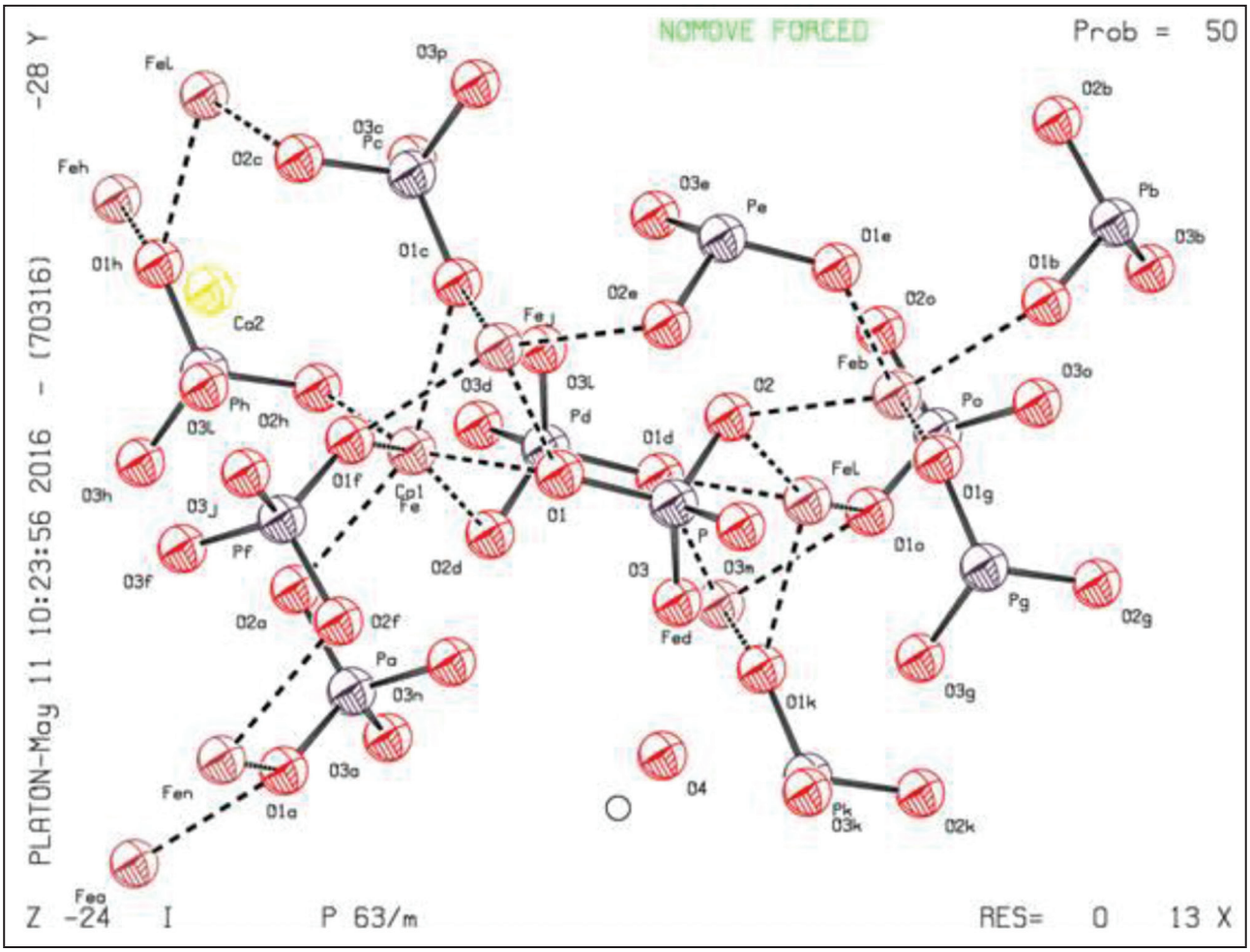

Figure 4: PLATON view of molecular structure of $Ca_{4.95}Fe_{0.05}(PO_4)_3OH$ compound showing Ca coordination in $Ca(1)O_9$ and P coordination in PO_4 polyhedron at 50% probability level.

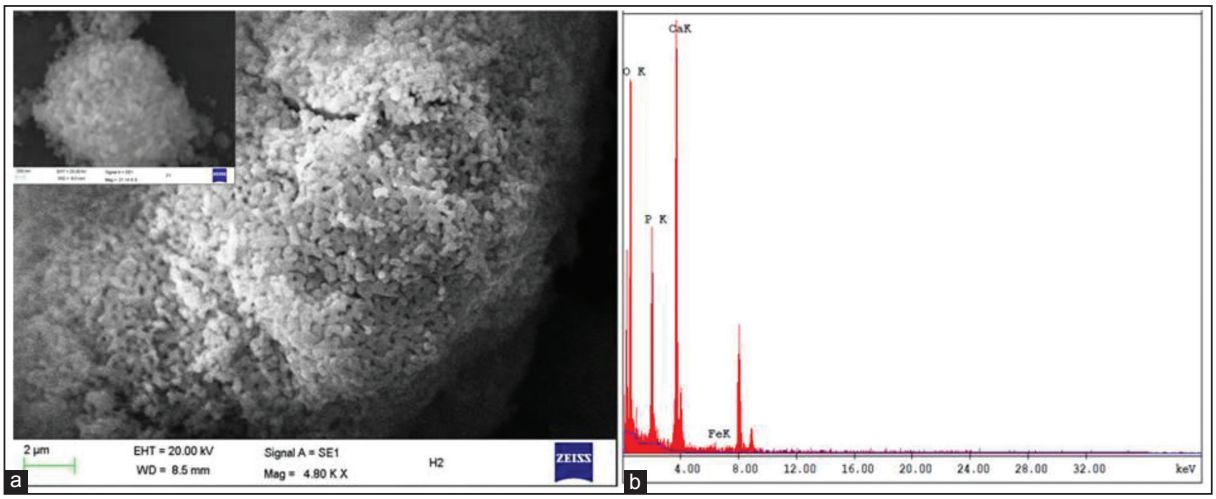

Figure: 5a and 5b. Scanning electron micrograph (left) and EDAX spectrum (right) of $Ca_{4.95}Fe_{0.05}(PO_4)_3OH$ powder.

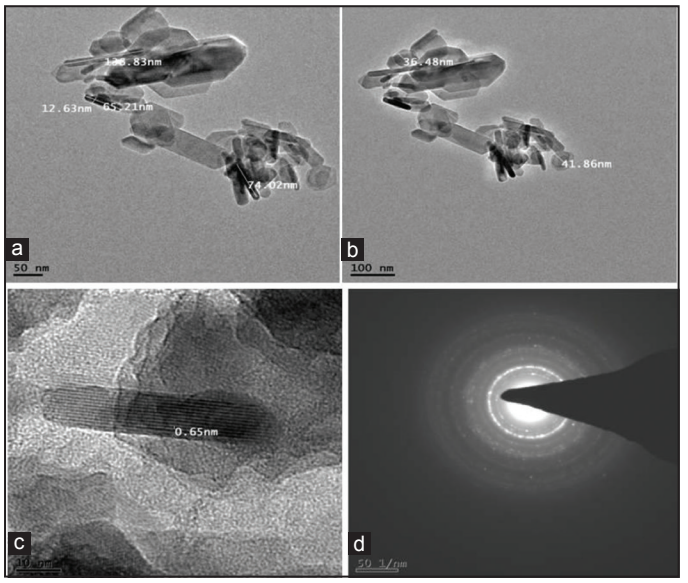

Figure 6: (a) and (b) TEM images (c) High resolution TEM picture and (d) SAED image of Sr-HA showing fundamental reflections.

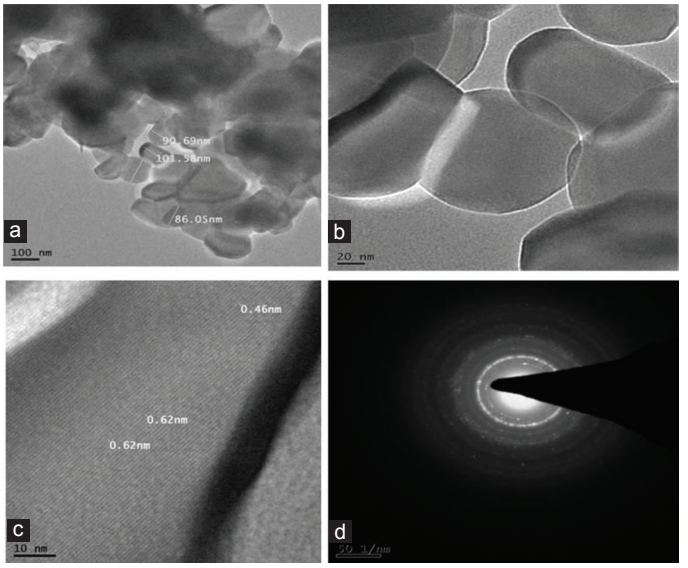

Figure 7: (a) and (b) TEM image of Fe-HA (c) HRTEM picture and (d) SAED image of Fe-HA showing fundamental reflections.

Table 5: Distribution of crystallite size (nm) along prominent reflecting planes of Sr- and Fe-substituted HA sample.

h k l	Crystallite size	
	(M=Sr)	(M=Fe)
0 1 0	19.51	78.07
0 1 1	26.17	62.83
1 1 0	19.77	39.36
0 2 0	26.41	79.14
1 1 1	79.36	63.41
0 0 2	28.98	63.71
0 0 2	32.03	63.77
0 1 2	32.09	64.08
2 1 0	26.91	64.19
1 2 1	29.45	53.84
1 1 2	54.13	53.9
0 3 0	16.3	54
0 2 2	27.53	54.16
0 3 1	55.28	65.08
122, 212	27.91	54.37
130, 10	24.05	55.07
131, 311	21.25	82.81
113	24.43	83.76
0 23	28.7	42.08
041, 222	28.82	84.63
132	21.73	42.52
230, 320	21.98	85.25
213	22.11	85.55
231, 321	22.41	85.9
410	45.23	86.18
42	22.78	86.47
141, 411	20.37	86.89
232	23.21	87.94
114	13.51	44.21
0 52	25.02	91.12
0 34	20.77	26.18
151	20.97	75.52

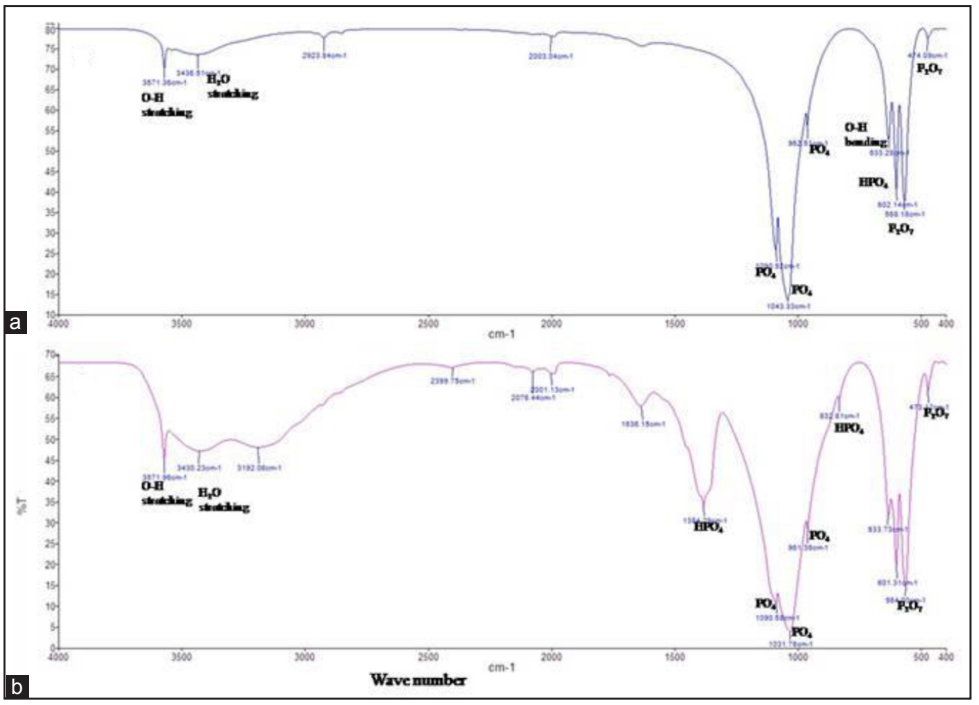

Figure 8: FTIR spectrum of (a) $Ca_{4.95}Sr_{0.05}(PO_4)_3OH$ and (b) $Ca_{4.95}Fe_{0.05}(PO_4)_3OH$ powders respectively.

4. CONCLUSIONS

The paper investigates a detailed structural analysis of Fe-HA and Sr-HA nanocrystals synthesized by a combination of hydroxide gel and hydrothermal technique. The title phases crystallize in hexagonal symmetry at room temperature. The refinement plots represent a good structure fit between observed and calculated intensities with satisfactory R-factors. The cell volume and Ca-O, P-O bond distances resister a slight decrease with the substitution of Sr and Fe in the parent HA matrix. The bond distortion in CaO_9 polyhedral increases, respectively, on Sr and Fe ions loading, but overall matrix structure remains intact. The nanocrystalline nature has been ascertained by X-ray diffraction data and high-resolution TEM micrographs. The XRD and TEM results show that the nanoparticles consist of two different chemical environments in materials having different chemical structure and bonding parameters. Thus, alteration of dimensions of nanocrystals (size/shape effect) and incorporation of chemical species in crystal structure change the structure and properties of the material in a remarkable manner.

5. ACKNOWLEDGMENTS

Authors thank the Department of Biotechnology, Government of India, for the award of visiting research professorship to one of the authors (OPS). We gratefully acknowledge the institutional support of Tezpur University, Assam, India, for hosting the DBT project in the Department of Chemical Sciences.

6. REFERENCES

1. A. Nakahira, S. Nakamura, M. Horimoto, (2007) Synthesis of modified hydroxyapatite substituted with Fe ion for DDS application, ***IEEE Transaction on Magnetic***, **43:** 2465-2467.
2. W. Pon-On, S. Meejoo, I. Tang, (2007) Incorporation of iron in to nano hydroxyapatite particles synthesized by microwave process, ***International Journal of Nanoscienc***, **6:** 9-16.
3. R. Morrissey, L. M. Rodriguez-Lorenzo, K. A. Gross, (2005) Influence of ferrous iron incorporation on the structure of hydroxyapatite, ***Journal of Materials Science: Materials in Medicine***, **16(5)**: 387-392.
4. H. K. H. Xu, L. E. Carey, S. Takagi, L. C. Chow, (2007) Premixed calcium phosphate cement: Synthesis, physical properties, and cell cytotoxicity, ***Dental Materials***, **23:** 433-441.
5. J. Kalitas, A. Bhardwaj, H. A. Bhatt, (2007) Nano crystalline calcium phosphate ceramics in biomedical engineering, ***Materials Science and Engineering C***, **27:** 441-449.
6. M. Okazaki, M. Taira, J. Takahashi, (1997) Rietveld analysis and Fourier maps of Hydroxyapatite, ***Biomaterial***, **18:** 795-799.
7. R. LeGeros, (2002) Properties of osteo conductive biomaterials: Calcium phosphate, ***Clinical Orthopaedics and Related Research***, **395:** 81-98.
8. R. LeGeros, S. Lin, R. Rohanizadeh, D. Mijares, J. LeGeros, (2003) Biphasic calcium phosphate bioceramics: Preparation, properties and applications, ***Journal of Materials Science: Materials in Medicine***, **14:** 201-209.
9. K.A.Cross,R.Jackson,J.D.Cashion,L.M.Rodriguez-LorenzoL.M, (2002) Iron substituted hydroxyapatite: Are soursable biomaterial with potential magnetic properties, ***European Cells and Material***, **3(2)**: 114-117.
10. C. Hou, S. Hou, Y. Hsueh, J. Lin, H. Wu, F. Lin, (2009) The *in vivo* performance of biomagnetic hydroxyapatite nanoparticles in cancer hyperthermia therapy, ***Biomaterials***, **30(23-24)**: 3956-3960.
11. F. P. Filho, M. P. F. Graça, R. E. Q. Nogueira, M. A. Valente, (2008) Structural and mechanical study of the sintering effect in hydroxyapatite doped with iron oxide, ***Physica B: Condensed Matter***, **403(19-20)**: 3826-3829.
12. O. Kuda, N. Pinchuk, L. Ivanchenko, O. Parkhomey, O. Sych, M. Leonowicz, R. Wroblewski, (2009) Effect of Fe_3O_4, Fe and Cu doping on magnetic properties and behavior in physiological solution of biological hydroxyapatite/glass composites, ***Journal of Materials Processing Technology***, **209(4)**: 1960-1964.
13. Y. Li, C. T. Nam, C. P. Ooi. (2009) Iron(III) and Mn(II) substituted hydroxyapatite nanoparticles: Characterization and cytotoxicity

analysis, ***Journal of Physics:*** **Conference Series**, **187:** 1-8.
14. J. Pena, M. V. Regi, (2003) Hydroxy apatite, tricalcium phosphate and biphasic materials prepared by a liquid mix method, ***Journal of the European Ceramic Society***, **23:** 1687-1696.
15. International Table of Crystallography, JCPDS-ICD Card Number 9-0432.
16. J. Laugier, B. Bochu. Laboratoire des Materiauxet du Genie Physique Ecole Nationale Superieure de Physique de Grenoble (INPG), Saint Martin d'Heres, France: Domaine Universitaire, BP 46, p38402.
17. H. M. Rietveld, (1969) A profile refinement method for nuclear and magnetic structure, ***Acta Crystallographica***, **2:** 65-71.
18. A. C. Larson, R. B. Von Dreele, (2004) General Structure Analysis System (GSAS), LANSCE, MS-H805, Los Alamos National Laboratory Report LAUR, p. 86.
19. H. Kojitani, M. Kido, M. Akaogi, (2005) Rietveld analysis of new high pressure strontium silicate $SrSi_2O_5$, ***Physics and Chemistry of Minerals***, **32:** 290.
20. A. R. West, (2003) In: N. Shah, T. A. V. Ress, Eds. Solid State Chemistry and its Application. Singapore: John Willey and Sons, p710-715.
21. D. Gopi, S. Nithiya, E. Shinyjoy, L. Kavitha, (2012) Molecular and biomolecular spectroscopy, ***Spectrochimica Acta Part A***, **92:** 194.
22. C. Yang, P. Yang, W. Wang, S. Gai, J. Wang, M. Zhang, J. Lin, (2009) Synthesis and characterization of Eu-doped hydroxyapatite through a microwave assisted microemulsion process, ***Solid State Sciences***, **11:** 1923.
23. N. P. Jagadalea, P. P. Jagtap, S. R. Bamane, (2015) Synthesis, characterization and *in vitro* drug delivery of nanostructured Fe-doped hydroxyapatite bioceramics, Pelagia Research Library, ***Der Chemica Sinica***, **6(6)**: 28-36.
24. K. M. T. Ereiba, A. G. Mostafa, G. A. Gamal, A. H. Said, (2013) *In vitro* study of iron doped hydroxyapatite, ***Journal of Engineering and Computer Sciences***, **6(2)**: 131-144.
25. R. N. Panda, M. F. Hsieh, R. J. Chung, T S. Chin, (2003) FTIR, XRD, SEM and solid state NMR investigations of carbonate containing hydroxyapatite nano-particles synthesized by hydroxide gel technique, ***Journal of Physics and Chemistry of Solids***, **64:** 193-199.
26. S. M. M. Arsad, M. L. Pat, (2011) In 2nd International Conference on Biotechnology and Food Science, Vol. 7. Singapore: IPCBEE, IACSIT Press.

****Bibliographical Sketch***

Prof O. P. Shrivastava - MSc (Physical Chemistry), PhD, Publications: Over sixty, Positions-Ex visiting professor, department of Chemistry, Tezpur university Assam, Former-Head, department of Chemistry and Dean, School of Biological and Chemical Sciences, Dr H. S. Gour Central University, Sagar, India. Awarded one USSR patent on 'Solid State Sensor of Sulphur dioxide (SO_2) in air'. Life member of Indian Chemical Society, Kolkata, Indian Science Congress Association, Kolkata, Indian Association of Solid State Chemists and Allied Scientist Jammu, Indian Association of nuclear Chemists and Allied Scientist, B.A.R.C. Bombay, India and Mineral Subcommittee International Centre for Diffraction Data (ICDD)..

APPENDIX

Appendix 1: Selected h, k, and l values, observed and calculated structure factors, d-spacing, and % intensity, respectively, of $Ca_{5-x}M_x(PO_4)_3OH$ (M=Sr and Fe, x=0.05) compounds. The reflection selected from the CIF output of the final cycle of the refinement.

h	k	l	F^2obs	F^2calc	d-spacing	Intensity %
0	1	0	435.045	426.353	8.15412	20.06
0	1	0	435.169	426.353	8.15412	9.98
0	1	1	136.997	130.168	5.25677	4.82
0	1	1	135.672	130.168	5.25677	2.38
0	2	0	1123.935	1112.361	4.07706	12.69
0	2	0	1113.307	1112.361	4.07706	6.26
1	1	1	389.388	375.890	3.88463	7.49
1	1	1	388.950	375.890	3.88463	3.72
0	2	1	218.386	139.036	3.50699	3.32
0	0	2	19042.123	19149.613	3.43825	44.13
0	0	2	18560.584	19149.613	3.43825	21.41
0	1	2	1078.272	1087.416	3.16812	13.17
0	1	2	1089.197	1087.416	3.16812	6.61
2	1	0	4021.999	3806.748	3.08197	24.86
2	1	0	4042.060	3806.748	3.08197	12.42
2	1	1	10209.219	10002.980	2.81242	100.00
2	1	1	10196.819	10002.980	2.81242	49.66
1	2	1	4218.806	4137.998	2.81242	41.53
1	2	1	4214.370	4137.998	2.81242	20.63
0	3	0	18754.512	18736.156	2.71804	86.50
0	3	0	18603.479	18736.156	2.71804	42.68
1	1	2	7043.617	6912.242	2.77659	64.82
1	1	2	7044.343	6912.242	2.77659	32.23
0	2	2	3725.718	3670.021	2.62839	29.29
0	2	2	3708.557	3670.021	2.62839	14.50
0	3	1	746.314	654.851	2.52774	5.53
0	3	1	756.602	654.851	2.52774	2.79
3	1	0	2269.162	2235.052	2.26155	6.74
3	1	0	2263.719	2235.052	2.26155	3.34
2	1	2	950.020	798.934	2.29494	5.31
2	1	2	953.267	798.934	2.29494	2.65
1	3	0	7784.671	7521.757	2.26155	22.48
1	3	0	7764.129	7521.757	2.26155	11.14
2	2	1	409.897	408.176	2.22703	2.40
1	3	1	1035.589	1183.855	2.14834	5.54
1	3	1	1076.301	1183.855	2.14834	2.86
1	1	3	1399.997	1191.368	2.06087	5.99
1	1	3	1334.636	1191.368	2.06087	2.84
0	2	3	1161.562	1274.164	1.99804	4.62
0	2	3	1183.352	1274.164	1.99804	2.34

(Contd...)

Appendix 1: *(Continued)*

h	k	l	F^2obs	F^2calc	d-spacing	Intensity %
2	2	2	9674.917	10394.930	1.94231	38.92
2	2	2	10054.169	10394.930	1.94231	20.05
3	1	2	1965.268	1936.647	1.88945	7.23
3	1	2	1925.093	1936.647	1.88945	3.52
1	3	2	3037.345	2984.127	1.88945	11.30
1	3	2	2974.187	2984.127	1.88945	5.50
2	3	0	2910.639	2847.544	1.87068	5.45
2	3	0	2952.194	2847.544	1.87068	2.74
4	1	0	3720.806	3666.877	1.77937	6.14
4	1	0	3701.900	3666.877	1.77937	3.03
2	1	3	9077.999	8790.069	1.83925	30.57
1	2	3	3955.443	3815.665	1.83925	13.41
2	1	3	9312.909	8790.069	1.83925	15.56
1	2	3	4053.941	3815.665	1.83925	6.82
3	2	1	3421.214	3404.714	1.80508	11.75
3	2	1	3437.972	3404.714	1.80508	5.86
2	3	1	3365.746	3350.683	1.80508	11.58
2	3	1	3381.703	3350.683	1.80508	5.78
0	4	2	5438.400	5591.778	1.75349	17.10
0	4	2	5523.693	5591.778	1.75349	8.62
1	4	0	5860.025	5816.128	1.77937	4.87
1	4	0	5889.898	5816.128	1.77937	9.86
0	0	4	38455.25	41985.33	1.71912	17.62
0	0	4	39118.41	41985.33	1.71912	8.89
3	2	2	2770.613	3490.944	1.64321	7.34
3	2	2	2880.232	3490.944	1.64321	3.78
1	3	3	1076.588	1058.250	1.60987	2.64
3	1	3	1064.932	1046.958	1.60987	2.54
4	1	2	936.351	842.141	1.58029	2.29
2	4	0	5606.553	5589.755	1.54098	6.41
2	4	0	5430.149	5589.755	1.54098	3.09
3	3	1	2182.510	2206.426	1.52993	4.89
3	3	1	2284.021	2206.426	1.52993	2.54
5	1	0	2159.583	2097.072	1.46452	2.21
2	4	1	2201.542	1925.661	1.50369	4.71
1	2	4	1483.913	1265.358	1.50135	2.89
0	5	2	6277.646	6364.546	1.47348	12.55
2	4	1	2275.908	1925.661	1.50369	2.41
0	5	2	6390.838	6364.546	1.47348	6.34
2	1	4	1293.245	1092.732	1.50135	2.63
5	1	1	5184.324	4975.537	1.43240	9.80
0	3	4	6643.965	6641.734	1.45290	12.24
5	1	1	5200.686	4975.537	1.43240	4.88

(Contd...)

Appendix 1: *(Continued)*

h	k	l	F^2obs	F^2calc	d-spacing	Intensity %
0	3	4	6676.644	6641.734	1.45290	6.11
3	2	3	3775.626	3756.668	1.44929	7.02
3	2	3	3756.916	3756.668	1.44929	3.47
3	3	2	1179.464	1130.688	1.42760	2.26
5	2	0	4561.913	4795.311	1.30570	3.36
4	3	1	3328.489	3257.480	1.31576	4.99
4	3	1	3279.229	3257.480	1.31576	2.45
5	2	1	1472.726	1386.734	1.28278	2.10
2	4	3	3492.295	3219.994	1.27885	4.74
2	4	3	3401.603	3219.994	1.27885	2.30
0	6	2	1542.075	1399.601	1.26387	2.17
2	1	5	4274.482	3625.513	1.25592	5.33
1	2	5	1623.213	1377.640	1.25592	2.03
2	1	5	4221.327	3625.513	1.25592	2.62
3	4	2	2209.300	1969.342	1.24896	2.88
5	1	3	3991.456	3963.727	1.23413	5.11
4	1	4	1901.637	1869.201	1.23636	2.36
1	4	4	4185.087	4116.251	1.23636	5.23
1	4	4	4079.338	4116.251	1.23636	2.54
2	5	2	5393.315	5474.792	1.22065	6.83
2	5	2	5210.071	5474.792	1.22065	3.29
4	4	0	4881.188	5206.495	1.17695	2.99
4	3	3	4250.903	3810.132	1.15717	4.68
4	3	3	4242.489	3810.132	1.15717	2.33
2	4	4	3082.794	2600.164	1.14747	3.34
5	1	4	3297.419	2677.689	1.11483	3.42
1	1	6	5644.197	4458.083	1.11356	5.53
1	1	6	5143.675	4458.083	1.11356	2.53
2	3	5	2064.299	2008.379	1.10807	2.10
5	3	2	3173.287	3484.442	1.10327	3.41
3	5	2	3186.396	3487.629	1.10327	3.44
M=Fe						
0	1	0	398.131	395.339	8.14713	17.93
0	1	0	399.031	395.339	8.14713	8.94
0	1	1	137.696	131.596	5.25270	5.13
0	1	1	159.027	131.596	5.25270	2.93
1	1	0	143.089	119.931	4.70374	2.17
0	2	0	982.023	1033.934	4.07356	11.07
0	2	0	1034.674	1033.934	4.07356	5.78
1	1	1	406.508	393.497	3.88147	8.09
1	1	1	452.418	393.497	3.88147	4.46
0	2	1	180.313	143.954	3.50411	2.85
0	0	2	19539.859	19417.21	3.43579	51.19
0	0	2	18646.61	19417.21	3.435	24.34
0	1	2	1307.024	975.134	3.16579	17.52

(Contd...)

Appendix 1: *(Continued)*

h	k	l	F^2obs	F^2calc	d-spacing	Intensity %
0	1	2	1054.017	975.134	3.16579	7.12
2	1	0	3414.995	3569.015	3.07932	21.48
2	1	0	3330.473	3569.015	3.07932	10.44
1	2	1	4026.697	4092.280	2.81007	41.29
2	1	1	9803.173	9962.083	2.81007	100.00
1	2	1	4008.881	4092.280	2.81007	20.45
2	1	1	9759.818	9962.083	2.81007	49.52
1	1	2	6555.602	6600.663	2.77446	66.66
1	1	2	6711.165	6600.663	2.77446	33.89
0	3	0	18786.037	18598.781	2.71571	88.43
0	3	0	17721.723	18598.781	2.71571	41.61
0	2	2	3505.443	3686.824	2.62635	30.37
0	2	2	4203.476	3686.824	2.62635	18.02
0	3	1	1064.481	714.428	2.52562	8.24
0	3	1	1093.079	714.428	2.52562	4.21
2	1	2	1265.005	877.000	2.29311	7.80
2	1	2	1304.801	877.000	2.29311	4.00
3	1	0	2314.313	2198.950	2.25961	7.17
1	3	0	9136.101	8705.616	2.25961	27.62
1	3	0	9046.035	8705.616	2.25961	13.60
3	1	0	2288.032	2198.950	2.25961	3.53
2	2	1	422.808	381.445	2.22515	2.62
1	3	1	1264.119	1158.526	2.14653	7.13
1	3	1	1175.183	1158.526	2.14653	3.31
1	1	3	1303.924	1325.605	2.05934	6.56
1	1	3	1152.500	1325.605	2.05934	2.89
0	4	0	2136.789	631.288	2.03678	2.57
0	2	3	999.939	1447.314	1.99654	4.70
0	2	3	970.684	1447.314	1.99654	2.27
2	2	2	9671.963	10418.844	1.94074	43.50
2	2	2	10189.649	10418.844	1.94074	22.72
1	3	2	2795.737	2994.666	1.88791	11.74
3	1	2	1872.144	2002.860	1.88791	7.76
1	3	2	2972.088	2994.666	1.88791	6.18
3	1	2	1987.756	2002.860	1.88791	4.09
2	3	0	3450.088	2846.418	1.86908	6.96
2	3	0	3570.915	2846.418	1.86908	3.58
2	1	3	8953.191	8988.851	1.83784	35.60
1	2	3	3780.932	3794.822	1.83784	15.15
2	1	3	9004.900	8988.851	1.83784	17.79
1	2	3	3804.764	3794.822	1.83784	7.58
2	3	1	3450.188	3329.556	1.80355	13.10
3	2	1	3559.679	3434.890	1.80355	13.48
3	2	1	3457.267	3434.890	1.80355	6.52
2	3	1	3350.555	3329.556	1.80355	6.34

(Contd...)

Appendix 1: *(Continued)*

h	k	l	F^2obs	F^2calc	d-spacing	Intensity %
4	1	0	4451.142	3761.761	1.77785	8.00
1	4	0	6689.573	5661.268	1.77785	12.19
4	1	0	4549.278	3761.761	1.77785	4.06
1	4	0	6834.892	5661.268	1.77785	6.19
0	4	2	5135.513	5434.458	1.75206	18.46
0	4	2	4853.296	5434.458	1.75206	8.71
0	3	3	416.988	494.868	1.75090	0.71
0	0	4	44299.44	42843.20	1.71789	25.21
0	0	4	41609.73	42843.20	1.71789	11.81
3	2	2	2828.572	3577.995	1.64186	8.66
3	2	2	2980.670	3577.995	1.64186	4.52
3	1	3	1178.452	1167.348	1.60860	3.39
1	3	3	1029.870	1019.624	1.60860	3.04
0	5	1	906.796	710.962	1.58546	2.43
2	4	0	6532.628	5551.903	1.53966	8.51
2	4	0	5206.098	5551.903	1.53966	3.42
3	3	1	2016.670	2237.286	1.52863	5.28
3	3	1	2029.582	2237.286	1.52863	2.64
2	4	1	1883.753	1799.688	1.50241	4.75
1	2	4	1437.108	1285.359	1.50023	3.57
2	1	4	943.727	837.913	1.50023	2.49
2	4	1	2113.836	1799.688	1.50241	2.63
0	5	2	6955.027	6262.241	1.47225	16.52
0	5	2	6313.372	6262.241	1.47225	7.50
5	1	0	2160.929	1781.659	1.46327	2.58
0	3	4	5825.355	6170.212	1.45181	13.84
0	3	4	5971.081	6170.212	1.45181	7.04
3	2	3	3826.212	3955.537	1.44813	8.82
3	2	3	4045.996	3955.537	1.44813	4.62
5	1	1	5314.149	4823.613	1.43118	11.92
5	1	1	5098.003	4823.613	1.43118	5.70
3	3	2	960.722	900.299	1.42641	2.25
4	3	1	3047.859	3492.932	1.31464	2.82
5	2	0	4401.071	5323.477	1.30458	4.01

(Contd...)

Appendix 1: *(Continued)*

h	k	l	F^2obs	F^2calc	d-spacing	Intensity %
5	2	0	5327.683	5323.477	1.30458	2.39
5	2	1	1542.000	1407.126	1.28169	2.73
2	4	3	3661.342	3424.717	1.27781	6.40
2	4	3	3476.445	3424.717	1.27781	3.03
0	6	2	1229.729	1074.901	1.26281	2.21
1	2	5	1519.401	1301.312	1.25500	2.63
2	1	5	4058.551	3476.777	1.25500	6.99
2	1	5	4165.759	3476.777	1.25500	3.57
3	4	2	2582.631	2139.482	1.24791	4.26
3	4	2	2447.812	2139.482	1.24791	2.02
6	1	0	2591.923	2347.929	1.24242	2.16
1	4	4	4075.493	4105.235	1.23539	6.82
4	1	4	1958.139	1976.415	1.23539	3.25
5	1	3	3914.399	3862.512	1.23312	6.52
1	4	4	4 4093.578	4105.235	1.23539	3.41
5	1	3	3646.206	3862.512	1.23312	3.04
2	5	2	5769.253	5523.965	1.21962	9.31
2	5	2	5499.470	5523.965	1.21962	4.43
4	4	0	4707.399	4650.082	1.17594	3.67
4	3	3	3911.161	4335.717	1.15621	5.76
4	3	3	3978.483	4335.717	1.15621	2.92
2	4	4	2704.573	2439.914	1.14656	3.99
4	2	4	1691.490	1524.967	1.14656	2.49
0	0	6	11455.403	11281.523	1.14526	2.79
5	1	4	3397.575	2590.372	1.11394	4.76
1	1	6	5192.075	4273.087	1.11275	7.37
5	1	4	2830.624	2590.372	1.11394	2.00
1	1	6	4733.432	4273.087	1.11275	3.37
2	3	5	2002.749	2052.231	1.10722	2.85
3	5	2	3293.921	3336.566	1.10234	4.62
5	3	2	3685.965	3734.239	1.10234	5.13
0	7	2	1702.971	1725.846	1.10234	2.35
5	3	2	3206.589	3734.239	1.10234	2.25
3	5	2	2862.658	3336.566	1.10234	2.03

Intensities <2% were omitted. F^2=Structure factor.
CIF: Crystallographic information framework